



Redoximorphic Bt horizons of the Calhoun CZO soils exhibit depth-dependent iron-oxide crystallinity

Chunmei Chen¹ · Diego Barcellos¹ · Daniel D. Richter² · Paul A. Schroeder³ · Aaron Thompson¹ 

Received: 9 May 2018 / Accepted: 22 June 2018 / Published online: 6 July 2018
© Springer-Verlag GmbH Germany, part of Springer Nature 2018

Abstract

Purpose Iron (Fe) oxyhydroxides and their degree of ordering or crystallinity strongly impact the role that Fe plays in ecosystem function. Lower crystallinity phases are generally found to be more reactive than higher crystallinity phases as sorbents for organic matter and chemical compounds, as electron acceptors for organic matter mineralization or as electron donors for dysoxic respiration. We investigated Fe solid phase speciation as a function of soil depth in a redoximorphic upland soil profile.

Materials and methods We examined a redoximorphic upland soil profile, which displayed alternating Fe-enriched and Fe-depleted zones of the Bt horizons with platy structure from 56 to 183 cm depth at the Calhoun Critical Zone Observatory in South Carolina, USA. Redoximorphic Fe depletion and enrichment zones were sampled to enable a detailed investigation of Fe mineralogy during redox transformations. All samples were characterized by total elemental analysis, X-ray diffraction, and ⁵⁷Fe Mössbauer spectroscopy.

Results and discussion Total Fe in the Fe-enriched and Fe-depleted zones was 26.3 – 61.2 and 15.0 – 22.7 mg kg⁻¹ soil, respectively, suggesting periodic redox cycling drives Fe redistribution within the upland soil profile. The Mössbauer data clearly indicated goethite (56 – 74% of total Fe) and hematite (7 – 31% of total Fe) in the Fe-enriched zones, with the proportion of hematite increasing with depth at the expense of goethite. In addition, the overall crystallinity of Fe phases increased with depth in the Fe-enriched zones. In contrast to Fe-enriched zones, Fe-depleted zones contained no hematite and substantially less goethite (and of a lower crystallinity) but more aluminosilicates-Fe(III) (e.g., hydroxy-interlayered vermiculite, biotite, kaolinite) with XRD and Mössbauer data suggesting a shift from oxidized biotite-Fe(III) at depth to hydroxy-interlayered vermiculite plus low-crystallinity goethite in the Fe-depleted zones in the upper Bt.

Conclusions Our data suggest the varied crystalline states of hematite and goethite may be important for Fe reduction over long-term time scales. The persistence of low-crystallinity Fe phases in Fe depletion zones suggests that both dissolution and re-precipitation events occur in the Fe-depleted layers. These variations in Fe phase abundance and crystallinity within similar redoximorphic features suggest that Fe likely shifts ecosystem roles as a function of soil depth and likely has more rapid Fe cycling in the upper Bt horizons in upland soils, while serving as a weathering engine at depth.

Keywords ⁵⁷Fe Mössbauer spectroscopy · Fe mineralogy · Redox cycling · Soil depth · Upland · X-ray diffraction

Responsible editor: Zhaohui Wang

Electronic supplementary material The online version of this article (<https://doi.org/10.1007/s11368-018-2068-2>) contains supplementary material, which is available to authorized users.

✉ Aaron Thompson
AaronT@uga.edu

¹ Department of Crop and Soil Science, University of Georgia, Athens, GA 30602, USA

² Nicholas School of the Environment, Duke University, Durham, NC 27708, USA

³ Department of Geology, University of Georgia, Athens, GA 30602-2501, USA

1 Introduction

Iron (Fe) oxidation and reduction are driven by both biotic and abiotic processes and are closely linked to the biogeochemical cycling of carbon (C), phosphorus (P), nitrogen (N), and many other chemical elements. In redox-dynamic systems, Fe redox cycling regulates the mobility and bioavailability of nutrients and contaminants (Hassellöv and von der Kammer 2008; Borch et al. 2010; Li et al. 2012). Fe also plays an important role in organic matter (OM) preservation and mineralization (Roden and Wetzell 1996; Dubinsky et al. 2010; Taylor and Konhauser 2011; Lalonde et al. 2012; Chen et al. 2014). The importance of Fe redox cycling and its relationship to other element cycles has received its greatest attention in aquatic sediments and wetland soils (Lovley 1995; Thamdrup 2000; Weber et al. 2006; Cheng et al. 2010). However, Fe redox cycling can also affect OM decomposition, nutrient dynamics, and mineral weathering in relatively well-drained, upland soils (Peretyazhko and Sposito 2005; Richter et al. 2007; Fimmen et al. 2008; Dubinsky et al. 2010; Yang and Liptzin 2015; Hall et al. 2016b). Multiple Fe phases can be present in soils including Fe-aluminosilicates and a variety of Fe(III) (oxyhydr)oxides (hereafter termed as Fe(III) oxides) ranging from short-range-ordered (SRO) ferrihydrite or nano-crystalline goethite phases to well-crystalline minerals such as goethite and hematite (Cornell and Schwertmann 2003). Any given Fe(III) oxide phase can exhibit a range of crystallinity (Cornell and Schwertmann 2003; Thompson et al. 2006b, 2011; Vogelsang et al. 2016; Chen et al. 2017), which correlates with the mineral's particle size and surface area, the degree of OM or foreign ion associated with mineral (e.g., isomorphous substitution, Al^{3+} for Fe^{3+}), and the solubility of the phase. Such variations result in various reactivities of Fe(III) oxides (Postma 1993; Roden and Zachara 1996; Bonneville et al. 2009) and thus govern their influence on ecosystem biogeochemistry.

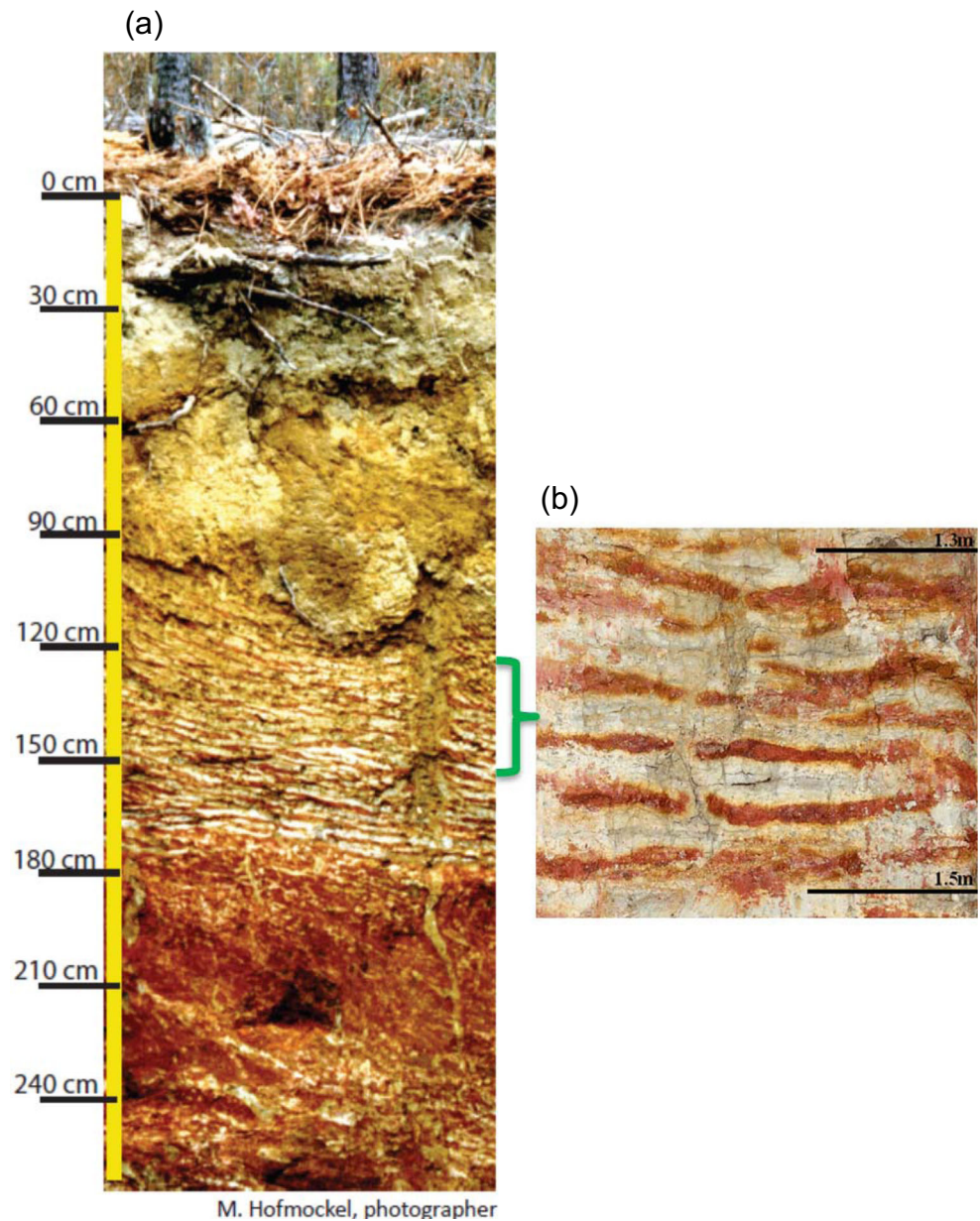
The chemical reactions and trajectories of Fe mineral differentiation depend on environmental redox conditions. Under anoxic to dysoxic conditions, even well-ordered Fe(III) oxide crystals are subjected to reductive dissolution (Bonneville et al. 2004, 2009). This process results in the formation of mobile Fe(II) (sometimes chelated by siderophores) in soil solution, which is transported within soils by both lateral and vertical diffusion. Fe(II) is rapidly oxidized and re-precipitated as Fe(III) oxides following contact with O_2 or to a much lesser extent other electron acceptors such as NO_3^- , SO_4^{2-} , and Mn(III). This re-precipitation, which depends on the temporal and spatial variability of soil moisture regimes and C availability, results in the formation of relatively “Fe-depleted” and “Fe-enriched” microsites with distinct redoximorphic features (Cornell and Schwertmann 2003;

Wiederhold et al. 2007; Fimmen et al. 2008; Mansfeldt et al. 2012). Redoximorphic soils are often influenced by strong redox fluctuations, which induce periodic dissolution and re-formation of Fe oxides. The mineral composition of soils subjected to alternating oxic and anoxic conditions has been investigated using a variety of techniques and found to be strongly influenced by the broader physiochemical properties (e.g., pH, Fe(II) concentrations, solution Al, Si or OM composition, bulk soil mineral composition, etc.) (Thompson et al. 2006b; Wiederhold et al. 2007; Fimmen et al. 2008; Thompson et al. 2011; Mansfeldt et al. 2012; Noël et al. 2014; Schulz et al. 2016; Vogelsang et al. 2016; Chen et al. 2017). SRO Fe minerals are often formed during oxidative precipitation at the oxic/anoxic interface in wetlands or when paddy surface soils are drained, likely because of the high OM content (Thompson et al. 2011; Kölbl et al. 2014; Vogelsang et al. 2016; Chen et al. 2017; Winkler et al. 2018). Conversely, Fe phases formed in the subsoil are typically more crystalline, likely due to the longer persistence of dissolved Fe(II) and its promotion of Fe(II)-catalyzed Ostwald ripening (Zhang et al. 2003; Thompson et al. 2006b; Cheng et al. 2009; Mansfeldt et al. 2012; Vogelsang et al. 2016).

Iron reduction and oxidation also appear to be relatively commonplace in many upland soils as evidenced by redoximorphic mottling (Veneman et al. 1998; Jacobs et al. 2002; Richter et al. 2007; Fimmen et al. 2008; Lindbo et al. 2010; Schulz et al. 2016). Several studies have documented Fe reduction in subsoils using morphological observations and geochemical analysis (Fimmen et al. 2008; Schulz et al. 2016). The combination of periodically perched water and/or root C inputs to clay-rich subsurface horizons appeared to promote Fe reduction and oxidation and generates prominent visual redoximorphic features indicative of Fe redox cycling that are strongly depth-dependent. Fe-depleted zones in upland soils have been found to be enriched in heavy Fe isotopes, whereas Fe-enriched zones exhibited enrichments of light Fe isotopes suggest that Fe-enriched microsites accumulate the light Fe preferentially mobilized from Fe-depleted microsites by reductive dissolution (Wiederhold et al. 2007; Mansfeldt et al. 2012; Bacon 2014; Schulz et al. 2016). Despite these observations, the impact of Fe reduction and oxidation on Fe mineralogy in upland redoximorphic soil is still not well explored (Fimmen et al. 2008; Schulz et al. 2016). Such knowledge is needed to understand the influence of the pedogenic redistribution process of Fe on the C dynamics and nutrient cycling in the terrestrial ecosystems.

Our objective is to use Mössbauer spectroscopy and X-ray diffraction to investigate Fe speciation and mineral composition as a function of soil depth along an upland soil profile, which displayed visible redoximorphic features. Separation of Fe-depleted zones (grayed stripes) and Fe-enriched zones (reddish stripes) during sampling (Fig. 1) enabled a detailed investigation of small-scale variations during redox transformations (Bacon 2014).

Fig. 1 **a** The sampled soil profile (0 to > 240 cm) at the Calhoun Critical Zone observatory (adapted from Fimmen et al. 2008). This soil profile has depth-dependent horizons that contrast in texture, mineralogy, structure, and biogeochemical process. **b** The subsurface horizons (e.g., 130–150 cm) displayed prominent visual redoximorphic features with distinct Fe-depleted zones (greyed stripes) and Fe-enriched zones (reddish stripes)



2 Materials and methods

2.1 Site descriptions and field sampling

The upland soil was excavated with a backhoe (> 2 m) in a granite-gneiss-derived Ultisol in the Calhoun Critical Zone observatory (CZO), Union County, SC, USA. The soil is of the Cataula series, derived directly from the underlying granite-gneiss bedrock, and has well-developed horizons including coarse-textured A and E horizons, acidic Bt horizons with prominent redoximorphic features and deep saprolite C horizons (Fimmen et al. 2008; Fig. 1). The soil and underlying weathering profile is ancient, estimated to have a residence time of > 2 million years (Bacon et al. 2012) and resides on

a geomorphically stable interfluvium with < 5% slope). The groundwater table fluctuates seasonally but is generally > 5 m depth, in what is now a subtropical-temperate climate. However, during winter and occasional summer rain events, the soil becomes epi-saturated above and within Bt horizons due to permeabilities that have saturated hydraulic conductivity (K_{sat}) measured at < 0.1 cm h⁻¹ from 100 to 200 cm depth (Table A1, Electronic Supplementary Material). The vegetation is dominated by loblolly pine (*Pinus taeda* L.) planted in 1975, after cotton cultivation for over a century (Richter et al. 2000). The soils are well studied in physical, biological, and chemical properties and in their dynamics of biogeochemical change at time scales of years to decades (e.g., Richter et al. 1994; Markewitz et al. 1998; Markewitz and Richter 2000;

Richter and Markewitz 2001; Richter et al. 2007; Li et al. 2008; Mobley et al. 2015). None of these previous studies have examined Fe mineralogy in its detail.

Depth-integrated, whole-horizon samples were taken from the A (0–15 cm) and E (15–45 cm) horizons, as no specific Fe-depleted and Fe-enriched zones could be identified because the whole soil matrix at these depths was depleted in Fe. The Bt horizon exhibited distinct redoximorphic features and was thus chosen for collecting the separate samples of the Fe-enriched and depleted zones. At Bt horizon, the depth-integrated samples of Fe-depleted and Fe-enriched samples were taken at 56–81, 81–107, 107–132, 132–158, and 158–183 cm. Fine roots and OM fragments were removed from the samples. Soil samples were air-dried and sieved with a 2-mm screen prior to analyses.

2.2 Total element and XRD analysis

The total soil elemental concentrations were measured by induction coupled plasma mass spectrometry (ICP-MS) following Li-metaborate fusion (Hossner et al. 1996) (Acme Labs, Vancouver, BC Canada). Loss and gain of Fe, Si, and Al were calculated using a simplified version of the open-chemical-system transport function (Chadwick et al. 1990), which ignores physical collapse and dilation of the soil column. The mass fraction of elements lost (or gained) from a soil horizon relative to the original elemental mass present in the parent material is calculated from the equation (Kurtz et al. 2000):

$$\tau_{m,w} = \left(\frac{C_{m,w}}{C_{m,p}} \times \frac{C_{i,w}}{C_{i,p}} \right) - 1 \quad (1)$$

where C is the concentration of an element (subscript m) in grams per kilogram, the subscript w refers to the weathered material, the subscript p refers to the parent material, and subscript i refers to the least mobile element. For the Gneiss parent material that underlies the Calhoun forest, we selected Ti as the least mobile element after comparing the relative abundance of Nb, Ti, and Zr. Fresh parent rocks were retrieved from the area near the Hansen Aggregate quarry located in Clinton, SC and the average of three used as the parent material for all horizons. Negative values of $\tau_{m,w}$ indicate loss of an element from that soil horizon, while positive values indicate enrichment.

Samples were analyzed for mineralogy by X-ray diffraction (XRD) using a Bruker D8 Advanced diffractometer. All samples were prepared by firmly pressing ground powder materials in the slides for bulk powder mounting (Moore and Reynolds 1997) and analyzed from 2° to 70° 2θ at a rate of 0.02° 2θ per second using $\text{CoK}\alpha$ radiation with an $\text{FeK}\beta$ filter. All data analysis was conducted in the EVA software package (Bruker).

2.3 ^{57}Fe Mössbauer spectroscopy

2.3.1 Mössbauer data collection

The Fe mineral composition of soils was assessed using ^{57}Fe Mössbauer spectroscopy collected at room temperature (RT, 295 K), 77 and 5 K. The ^{57}Fe Mössbauer spectra were recorded in transmission mode with a variable-temperature He-cooled cryostat (Janis Research Co.) and a 1024 channel detector. A ^{57}Co source (~ 50 mCi) embedded in an Rh matrix was used at room temperature. The velocity (i.e., γ -ray energy) was calibrated using α -Fe foil at 295 K, and all center shifts (CSs) and peak positions are reported with respect to this standard. The Mössbauer data for the bulk samples at A (0–15 cm) and E (15–45 cm) was not successfully collected due to very low Fe concentrations.

2.3.2 Mössbauer spectral analysis approach

Mössbauer spectral fitting was performed using the Voigt-based fitting method of Rancourt and Ping (1991) as implemented in the Recoil™ software. All fitting parameters are given in the Electronic Supplementary Material (Tables A2 to A6). The relative abundance of each Fe site population (e.g., mineral phase) was extracted from the spectral fitting as a fraction of the total Fe spectral area. All errors in Mössbauer fitting parameters are two-standard deviation (2σ) errors, as calculated by Recoil™. Quantifying Fe phase abundance in this manner assumes equal Mössbauer recoilless fractions of all detected phases; this assumption is expected to be valid at cryogenic temperatures and also to be a good approximation at least up to 295 K with dry samples (Lalonde et al. 1998; Rancourt 1998).

In Mössbauer spectra, each spectral component corresponds to one Fe-bearing solid phase or to a group of unresolved Fe-bearing solid phases. These components take the form of a doublet, sextet, octet (none resolved here), or a collapsed sextet—indicating a solid phase near its magnetic ordering temperature (T_N). Solid phases well above (doublet) or below (sextet) their T_N will not exhibit any vertical (i.e., count axis) distance between the peak troughs and the baseline. When Fe solid phases are near their T_N , they exhibit an intermediate shape between a doublet and full sextet, which fills the area between the upper baseline and the inverse troughs of the peaks. We approximate this by using a separate collapsed sextet component (i.e., a sextet with exceedingly large line widths and $B_{\text{hf}} = 0$ T).

Fe(III) oxides of lower crystallinity require lower measurement temperatures to magnetically order (and hence form a sextet) than Fe(III) oxides of higher crystallinity. The ordering temperature of Fe(III) oxides can be decreased by coprecipitation with OM (Schwertmann et al. 2005; Eusterhues et al. 2008; Mikutta et al. 2008; Chen et al.

2015), by small particle size, as well as by substitution of Fe by Si and Al (Murad and Schwertmann 1983; Schwertmann et al. 2004; Thompson et al. 2011). The area of Fe(III) sextet increases as the measurement temperature decreases since Fe(III) oxide phases of lower crystallinity—still represented by a doublet at a higher measurement temperature—are added to the respective sextet at the lower measurement temperature. The proportions of magnetically ordered Fe(III) oxide were quantified by the area of the respective Fe(III) oxide sextet measured at a certain temperature. Fe(III) oxide that have not yet ordered at a specific measurement temperature appears as either a collapsed feature or as part of the Fe(III) doublet in the Mössbauer spectrum. In the 5 K spectra, if we assume all the Fe(III) oxides have magnetically ordered, we can refine the Fe(III) quadrupole doublet to correspond to Fe(III) complexed with OM or in aluminosilicates. However, since total C concentrations in these samples are low (<0.3%), OM-complexed Fe(III) is unlikely. Therefore, we attributed the Fe(III) central doublet at 5 K to Fe(III) in the aluminosilicates. The Fe(III) sextets (goethite-like and hematite-like) would represent phases with clear distinctive similarity to goethite and hematite, whereas the most disordered Fe oxide phases would be represented by the partially collapsed Fe(III)

“sextet” having their superparamagnetic blocking temperatures near 5 K. No ferrous doublet was detected for any of the samples. We calculated the abundance of each Fe-bearing phase from the spectral area of each respective component in the 5 K spectra.

3 Results and discussion

We take advantage of the unique repeating horizontal sequence of enriched iron layers (Tyger stripes) to discern the influence of soil depth on the crystallinity and speciation of Fe minerals (Fig. 1).

3.1 Depth distribution of soil Fe speciation in Fe-enriched zones of the Bt horizons

Collection of Mössbauer spectra at RT (295 K), 77 K, and 5 K allows us to characterize the crystallinity-continuum of the Fe(III)-oxide solid phases in the samples (Figs. 2 and 3, A1, and A2). The more crystalline portions of Fe(III) oxides are magnetically ordered at higher temperatures (and hence form a sextet) than Fe(III) oxides of lower crystallinity. The

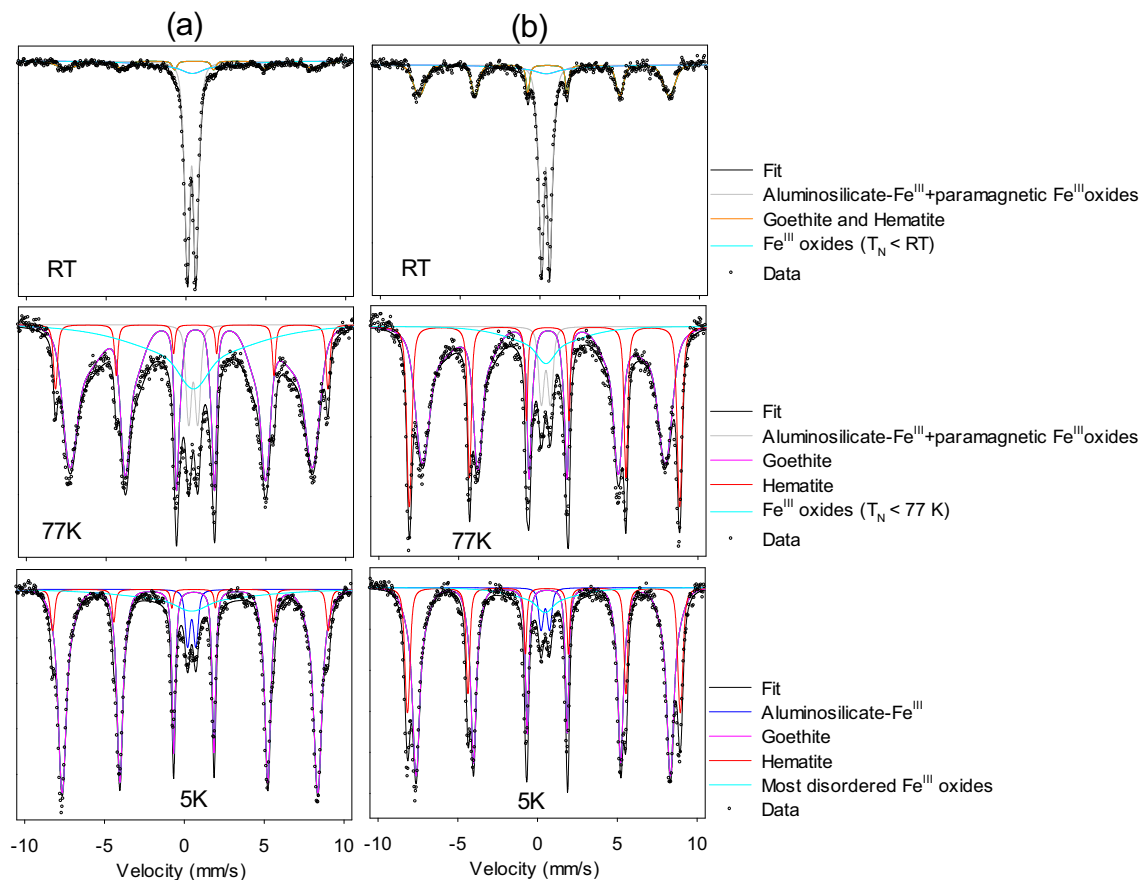


Fig. 2 Fitted Mössbauer spectra of Fe-enriched samples at room temperature (RT), 77 K, and 5 K at soil depth of **a** 56–81 cm and **b** 132–158 cm, respectively. The spectral fitting parameters are shown in the Appendix Tables A2–A4

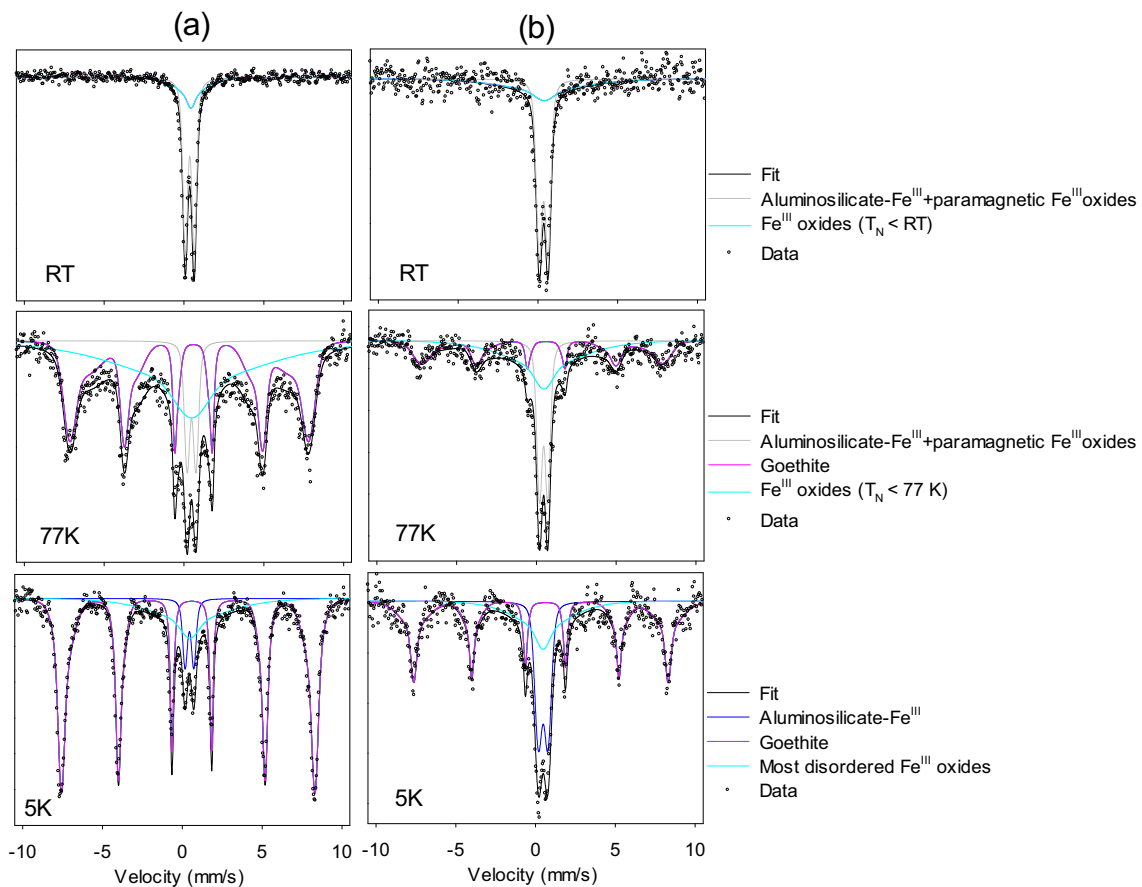


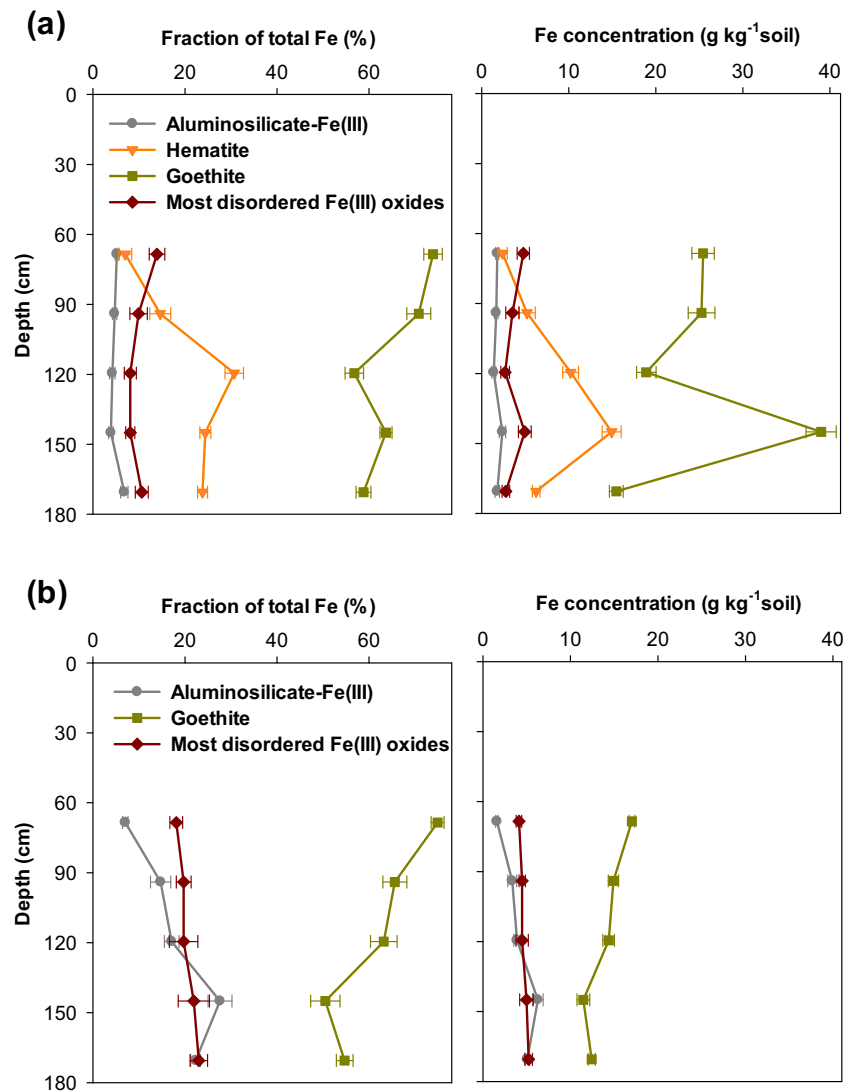
Fig. 3 Fitted Mössbauer spectra of Fe-depleted samples at room-temperature (RT), 77 K, and 5 K at soil depth of **a** 56 – 81 cm and **b** 132 – 158 cm, respectively. The spectral fitting parameters are shown in the Appendix Tables A5–A7

Mössbauer spectra of Fe-enriched soils at RT (295 K) were dominated by a Fe(III) doublet with a small sextet (Figs. 2 and A1, Electronic Supplementary Material). At RT, we can resolve only one sextet with parameters intermediate of hematite and goethite (Table A2, Electronic Supplementary Material), which is indicative of the presence of well-crystalline hematite and goethite (Murad and Cashion 2004; Thompson et al. 2011; Chen et al. 2017). With increasing soil depth, i.e., between 56 and 132 cm, we observed a general increase in Mössbauer spectral area of the RT-sextet relative to the central Fe(III) doublet for the Fe-enriched samples (Figs. 2 and A1 and Table A2, Electronic Supplementary Material), indicating that the well-crystalline large hematite and goethite is more abundant deeper in the profile.

Cooling the samples to 77 K generated increased sextet area with two distinct components relative to the doublet (Figs. 2 and A1, Electronic Supplementary Material). We were able to clearly identify goethite and hematite with similarly negative quadruple splitting (QS) value (-0.10 mm/s for goethite and -0.13 mm/s for hematite) and distinctive hyperfine field strength (B_{hf}) of $44.5 - 46.6$ and $52.4 - 52.9$ T at 77 K, respectively (Table A3, Electronic Supplementary Material). At 5 K, the relative spectral area of the hematite

($QS = \sim -0.1$ mm/s; $B_{\text{hf}} = \sim 53$ T) remained the same as at 77 K, and the goethite component ($QS = \sim -0.12$ mm/s; $B_{\text{hf}} = \sim 49$ T) has only slightly higher spectral area relative to 77 K spectra (3 – 10% difference) (Tables A3 and A4, Electronic Supplementary Material). This indicates all hematite and most goethite are magnetically ordered at 77 K or above. Fe(III) oxide phases that are blocked or near their blocking temperature at 5 K, which were modeled as a collapsed sextet, likely representing the most disordered Fe(III) oxide phases such as ferrihydrite or nanogoethite (Murad and Cashion 2004; Thompson et al. 2011; Chen et al. 2017). Fe(III) atoms in aluminosilicates are too distant from each other to order magnetically and thus produce a doublet at 5 K (Murad and Cashion 2004; Schwertmann et al. 2005; Thompson et al. 2011; Chen et al. 2017). Hence, when all Fe(III) oxides have ordered into a (collapsed) sextet at 5 K, the remaining doublet represents Fe(III) in aluminosilicates. In the Fe-enriched samples, the 5 K-doublet is a minor component of the spectra. In Fe-enriched zones, >90% of total Fe was hosted by Fe(III) oxides such as goethite (56 – 74%) with a much lower contribution of hematite (7 – 31%) and the most disordered Fe(III) oxides ($T_N < 5$ K) (8 – 14%) (Fig. 4).

Fig. 4 Fe fraction (% of total Fe) and concentration (g kg^{-1} soil) from Mössbauer spectroscopy along the depth gradient in the **a** Fe-enriched and **b** Fe-depleted zones, respectively. The fraction of each Fe-bearing group assignment was calculated from the proportional spectra area of the MBS-modeled components. Concentration was calculated by multiplying the fraction of spectral area for each phase in the Mössbauer spectrum by the total Fe



The ratio of magnetically ordered hematite and goethite measured at RT to those measured at 5 K increased with soil depth and reached maxima at depth of ~ 120 cm for Fe-enriched zones (Fig. 5); if we consider this ratio between sextets at 77 and 5 K, Fe-enriched samples below ~ 90 cm have a higher crystallinity ratio (77 K/5 K) than the soils near the top of the Bt. Taken together, this indicates that Fe(III) oxides in the Fe-enrichment zones closer to the top of the Bt horizon tend to have a lower crystallinity or smaller particle size, relative to Fe phases in the deeper soil profile. Although these subsoils have low C content ($< 0.3\%$), total C concentration closer to the top of the Bt horizon is slightly higher than that deeper in the soil profile (Fig. A3, Electronic Supplementary Material). In addition, soils near the top of the Bt have a much higher Si concentrations than deeper soils (Fig. 6). Previous studies have demonstrated that Si substituted in ferrihydrite structure or sorbed OM on ferrihydrite can result in a decrease in

ferrihydrite particle size and crystallinity (Eusterhues et al. 2008; Mikutta et al. 2008; Dyer et al. 2012; Cismas et al. 2014; Chen et al. 2015) and also prevent ferrihydrite transformation to more crystalline, thermodynamically stable forms (Schwertmann and Thalmann 1976; Mayer and Jarrell 1996; Jones et al. 2009; Chen et al. 2015). Goethite and hematite are considered thermodynamically more stable phases than ferrihydrite (Cornell and Schwertmann 2003). But it may be that like ferrihydrite, interactions between Si or OM and Fe retard the Ostwald ripening processes of goethite and hematite by blocking dissolution sites on the goethite and hematite or hindering the nucleation of more crystalline mineral phases (Schwertmann and Thalmann 1976; Schwertmann and Cornell 1991). Therefore, at a deeper depth, lower OM or Si concentrations may facilitate the formation of well-crystalline hematite and goethite during the Fe redox cycling likely in these soils. Thompson et al. (2011) observed the

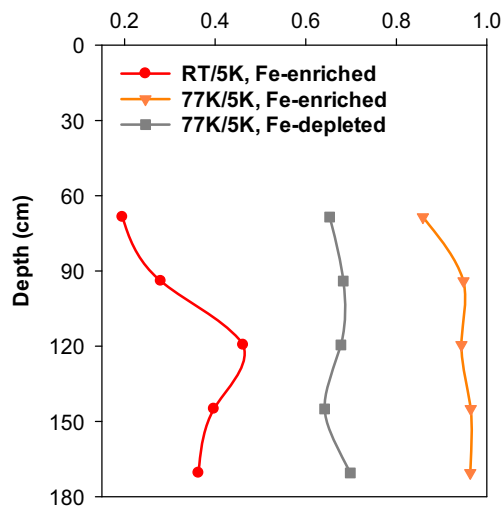


Fig. 5 Ratio of magnetically ordered Fe(III) oxides at room temperature (RT) and 77 K to Fe(III) oxides ordered at 5 K in the Fe-enriched and depleted zones, based on Mössbauer spectroscopy analysis for all soils studied. The abundance of the magnetically ordered Fe(III) oxides was derived from the spectral area of the sextet components in RT, 77 K, and 5 K spectra, respectively

accumulation of less-crystalline nanogoethite in soils with climates having relatively high rainfall and attributed this to the high concentration of OM in surface soils and Si or Ti in subsoils.

Iron reduction rates often scale with the crystallinity of Fe oxide phases, with less-crystalline oxides more available for microbial reduction (Roden and Zachara 1996; Roden and Wetzel 2002; Bonneville et al. 2009). Our data provided evidence that Fe(III) availability may decline with depth, potentially constraining Fe reduction. This supports a recent study, which showed that Fe reduction declined by two orders of magnitude below 1 m in an upland tropical soil likely due to the limited C availability, even though soil O_2 was lower at depth (Hall et al. 2016a).

Thus, we propose that Fe redox cycling and associated C and nutrient dynamics (Peretyazhko and Sposito 2005; Dubinsky et al. 2010; Buettner et al. 2014; Hall et al. 2016a, b) are likely more rapid near the top of the Bt than at depth and likely serves different roles in Critical Zone function. Clearly, the Fe-depleted and Fe-enriched zones at depth are direct evidence of Fe cycling, but their higher crystallinity (relative to the top of the Bt) suggests a different timescale of Fe redox cycling or suggest other processes—for instance Fe^{2+} -promoted re-crystallization—function to a greater degree at depth than near the surface.

3.2 Formation of goethite versus hematite during pedogenesis

We observed a proportional increase in hematite f_{tot-Fe} , coincident with a proportional decrease in goethite f_{tot-Fe} with increasing soil depth, while f_{tot-Fe} assigned to the aluminosilicate-Fe(III) and the most disordered Fe(III) oxides ($T_N < 5$ K) remained relatively uniform along the vertical soil profile (Fig. 4a). Due to a distinct enrichment peak in total Fe at a depth of ~ 150 cm (Fig. 6), the Fe concentration of all four Fe-bearing group assignments displayed maxima at this depth (~ 150 cm) (Fig. 4a). Because weathering of aluminosilicate minerals has probably produced goethite plus some hematite, the increasing percentage of hematite concomitant with a decrease in goethite along the vertical profile suggests potential pedogenic transformation of goethite to hematite. Hematite very rarely occurs as the sole oxide in a soil, but it is often associated with goethite (Cornell and Schwertmann 2003). The direct (solid-state) transformation of goethite to hematite at typical soil temperature and water activity may be thermodynamically favorable in certain circumstances, but it is kinetically inhibited (Langmuir 1971; Yapp 1983; Trolard and Tardy 1987) and it is not known to occur in natural

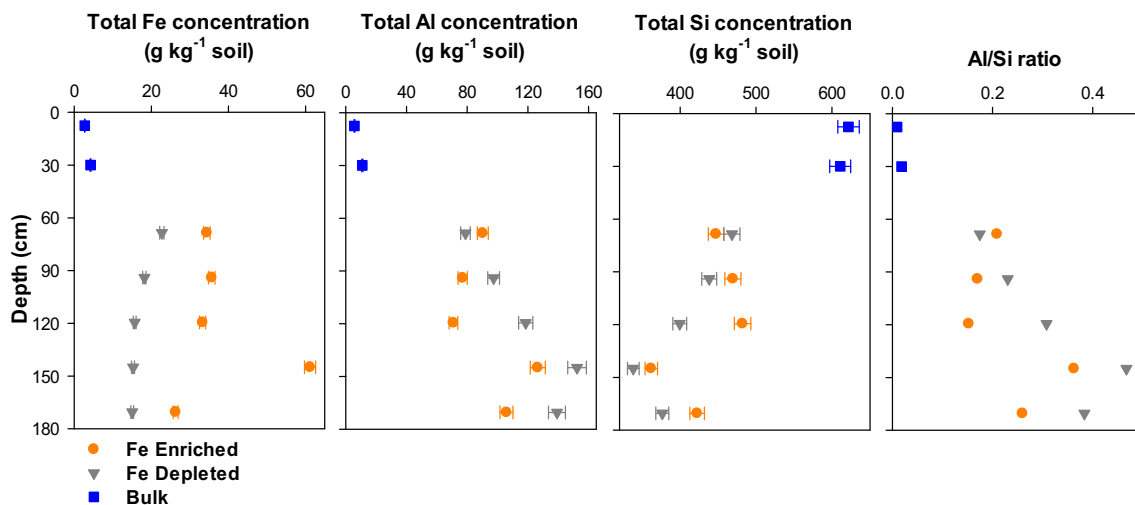


Fig. 6 Depth profiles of total Fe, Al, and Si concentrations and the Al/Si molar ratio in Fe-enriched and Fe-depleted zones in the subsurface and the bulk samples in the surface

environments. However, hematite can form under soil conditions from a ferrihydrite precursor (Bao and Koch 1999). Important factors influencing the relative proportions of hematite and goethite are temperature, moisture content, OM content, and other ions in solution (Schwertmann and Taylor 1989; Schwertmann 1985; Cornell and Schwertmann 2003). In this upland profile, soil saturated hydraulic conductivity (K_{sat}) largely dropped from $\sim 2.6 \text{ cm h}^{-1}$ at the near-surface E horizon to $\sim 0.5 \text{ cm h}^{-1}$ in the upper Bt horizon ($\sim 80 \text{ cm}$) and ~ 0.03 at 105 cm (Table A1, Electronic Supplementary Material). It is likely that water ponds above $\sim 105 \text{ cm}$ and thus soils in deeper horizon might be relative drier. Low moisture content may favor the dehydration of ferrihydrite to hematite (Torrent et al. 1982; Zhang et al. 1998), compared to transformation of ferrihydrite to goethite formation via Ostwald ripening. In addition, slightly lower OM content in deeper profile relative to the top Bt (Fig. A3) may also facilitate hematite formation rather than goethite formation (Kämpf and Schwertmann 1983).

A similar pattern of alternative Fe-enriched and Fe-depleted layers generated from the dissolution of reduced Fe forms (e.g., sulfides) has been documented to occur at depths of 100s of meters below the surface in large-scale kaolinite deposits local to the southeastern USA (Schroeder 2018; Schroeder et al. 1997, 2004). Phase characterization of the Ti- and Fe-bearing phases in these kaolinite-rich rocks revealed the transition from reduced Fe(II) clays, to Fe-enriched clays, to Fe-depleted clays, with the Fe-enriched clays dominated by hematite (although SRO nanogoethite or ferrihydrite would not have been detectable by XRD). This layering is often termed liesegang banding and observed in many different weathered rock types (Merino 1984). The patterns of Fe-enriched and Fe-depleted layers observed in the Bt horizons of the Calhoun CZO may in part reflect inherited distribution of Fe in the form of amphibole-rich foliations, which are then subsequently redistributed via redox cycling.

3.3 Depth distribution of soil Fe speciation in Fe-depleted zones in the Bt horizons

In the Fe-depleted zones, the only feature in the RT Mössbauer spectra was a paramagnetic doublet (Figs. 3 and A2, Electronic Supplementary Material), indicating a complete loss of well-crystalline large-size hematite and goethite. However, at 77 K, a considerable sextet structure was formed, with derived Mössbauer parameters ($QS = -0.09$ to -0.13 mm/s ; $B_{\text{hf}} = 43 - 45 \text{ T}$) (Table A6, Electronic Supplementary Material) consistent with goethite (no hematite sextet was detected, Figs. 3 and A2, Electronic Supplementary Material). As temperature decreased from 77 to 5 K, the relative area of the goethite sextet ($QS = -0.11$ to -0.13 mm/s ; $B_{\text{hf}} = 48.6 - 49.8 \text{ T}$) increased from 32 to 49% to 50 – 75% with a concurrent decrease in the central Fe(III) doublet area

(Figs. 3 and A2 and Tables A6 and A7, Electronic Supplementary Material), thus providing evidence that a considerable fraction of low-crystallinity nanogoethite ($< 8 \text{ nm}$) is present in these samples, because this phase exists as doublets at 77 K but as sextets at 5 K (Janot et al. 1973). In the Fe-depleted zones, 50 – 75% of the total Fe is contained in this low-crystallinity goethite, whereas aluminosilicate-Fe(III) and the most disordered Fe(III) oxides ($T_N < 5 \text{ K}$) accounted for 7 – 28 and 18 – 23% of total Fe, respectively (Fig. 4b). The ratio of magnetically ordered goethite measured at 77 K to that measured at 5 K showed little variation with soil depth (Fig. 5). Therefore, unlike the Fe-enriched zones, the crystallinity of goethite is less affected by soil depth in Fe-depleted zones. With depth, the proportion and concentration of the most disordered Fe(III) oxides ($T_N < 5 \text{ K}$) did not exhibit a significant trend (Fig. 4b). However, both the percentage and concentration of aluminosilicate-Fe(III) increased with soil depth, concurrent with a decrease in the proportion and concentration of goethite (Fig. 4b). The deeper Bt horizons were enriched in aluminosilicate-Fe(III), with corresponding depletion of low-crystalline goethite. We observed similar fitting parameters of the aluminosilicate-Fe(III) doublet for all the samples. The aluminosilicate-Fe(III) doublet at 5 K has a CS value of 0.44–0.48 mm/s and a QS value of 0.54 – 0.60 mm/s (Tables A4 and A7, Electronic Supplementary Material), typical of octahedral Fe(III) substituted in aluminosilicates (Dyar et al. 1987; Murad and Cashion 2004). Mössbauer parameters of the aluminosilicate-Fe(III) in this study are similar to that reported for subsurface sediments containing illite/muscovite/vermiculite (Kukkadapu et al. 2006), the kaolinite/halloysite-rich subsurface soils (Thompson et al. 2011), and vermiculite/illite/kaolinite-bearing wetland soils (Chen et al. 2017). XRD displayed the dominance of kaolinite with less presence of hydroxyl-interlayered vermiculite- and biotite-like aluminosilicates in these soils (Figs. A4 and A5, Electronic Supplementary Material). The Fe(III) could substitute in any of these aluminosilicate phases and all exhibit similar Mössbauer parameters (Greenwood and Gibb 1971; Fysh et al. 1983), consistent with our observations. In the Fe-depleted zones, total Si concentration generally decreased with soil depth; however, total Al increased with depth (although both remained a net loss relative to parent rock, see Fig. A6, Electronic Supplementary Material), leading to an increasing Al/Si ratio with soil depth (Fig. 6). Increasing Al/Si ratios are due to the pedological processes of lessivage (Quénard et al. 2011), which results in a substantial vertical transfer of fine particles with mainly aluminosilicates from A and eluvial E horizons to an illuvial Bt horizon. Consequently, lessivage caused strong enrichment of quartz in the near-surface A and E horizons. XRD showed relatively more secondary aluminosilicate clay minerals including kaolinite and biotite in the deeper soil profile (Fig. A4, Electronic Supplementary Material), which may contribute to the

enrichment of aluminosilicate-Fe(III) in the deeper soil profile. In addition, we do see strong evidence of the depth-dependent weathering of biotite to vermiculite in these soils (see Section 4 of the Appendix and Figs. A4 and A5) with oxidized biotite present at the deepest Bt horizons being replaced by vermiculite in the Fe-depleted Bt horizons near the top of the Bt.

3.4 Differences in Fe speciation between Fe-enriched and depleted zones of the Bt horizons

There was significantly more Fe in the enriched Bt horizons than in the depleted zones (26.3 – 61.2 and 15.0 – 22.7 mg Fe kg⁻¹ soil in Fe-enriched and Fe-depleted zones, respectively, Fig. 6). Many have proposed that differentiation between the Fe-enriched and depleted zones reflects mobilization of Fe(III) between adjacent layers [i.e., diffusion and leaching of Fe from the depleted zones coupled to precipitation in the enriched zones] (Richter et al. 2007; Wiederhold et al. 2007; Fimmen et al. 2008; Mansfeldt et al. 2012; Bacon 2014; Schulz et al. 2016). Despite lower total Fe concentrations, the depletion zones contained more aluminosilicate-Fe(III) than the Fe-enriched zones (Fig. 4). XRD detected vermiculite-like minerals in the depleted zones (Fig. A4, Electronic Supplementary Material) but not in the enriched zones (Fig. A5, Electronic Supplementary Material). In addition, Al/Si ratio was higher in the depleted zones than in the enriched zones, largely driven by inverse trends in Al and Si with depth in the depleted zones (Fig. 6). Fe-depleted zones contained more clay-sized particles than Fe-enriched zones (Fimmen et al. 2008). These differences may result from particle sorting associated with colloid dispersion/coagulation during Fe reduction and oxidation events (Thompson et al. 2006a; Fimmen et al. 2008) and synthesis and precipitation of clay minerals.

The concentration of hematite-Fe in the enriched zones ranged from 2.4 to 10.9 g kg⁻¹, whereas no hematite was detected in depleted zones (Fig. 4). Goethite-Fe concentrations ranged from 15.5 to 40.0 g kg⁻¹ in the enriched zone but decreased to 11.5 – 17.0 g kg⁻¹ in the depleted zone. Both Fe-enriched and depleted zones had ~60% of total Fe as goethite phases of variable crystallinity. If we assume that the protolith oxidatively weathered to secondary Fe(III) oxides that eventually transformed to crystalline goethite and hematite, these results would suggest a complete reductive dissolution of hematite and partial dissolution of goethite in the depleted zone, along with the mobilization of Fe(II) via diffusion and water percolation and its subsequent oxidation and precipitation to Fe(III) oxides in adjacent, more oxidizing sites that become enriched in Fe. Iron depletion under O₂-limited pedogenesis is predominantly mediated by dissimilatory Fe reducing bacteria, which are able to use Fe(III) oxides as alternate terminal electron acceptors (Lovley et al. 2004). The

reducibility of crystalline Fe(III) oxides like goethite and hematite is much lower than that of SRO Fe(III) oxides like ferrihydrite (Postma 1993; Roden and Zachara 1996; Bonneville et al. 2009). Therefore, previous studies emphasize that SRO Fe phases play a central role in sustaining soil Fe redox cycling in the critical zone and any associated impacts on C or nutrient dynamics (e.g., Hall et al. 2016b; Ginn et al. 2017; Barcellos et al. 2018). However, we conclude that crystalline Fe phases of both hematite and goethite may also be important for Fe reduction, especially over long-term timescales.

We noted that the goethite in the Fe-depleted zones has a lower crystallinity than the average goethite in the Fe-enriched zones (Figs. 2, 3, and 5). This observation is unexpected, as lower crystallinity Fe phases should be reductively dissolved preferentially relative to more crystalline phases (Postma 1993; Roden and Zachara 1996) and result in selective retention of more kinetically stable, large crystalline goethite in the Fe-depleted zones. Therefore, we surmise that selective dissolution alone does not govern the composition of iron in these profiles and instead regeneration and re-precipitation reactions are critical. Periods of reducing conditions are ephemeral within the Fe-depleted zones, and O₂ associated with prominent drying events may well help oxidize residual Fe(II) that is likely sorbed onto soil surfaces in the Fe-depleted zone. Since these depleted zones have a much higher OM content than the Fe-enriched zones (Fig. A3), this is likely to favor the regeneration of low-crystallinity nanogoethite (Chen and Thompson 2018) relative to more crystalline phases and also to inhibit the further ripening of nanogoethite to well-crystalline large goethite. In fact, the regeneration of low-crystallinity nanogoethite in the Fe-depleted zone may accelerate subsequent Fe reduction when reducing conditions re-establish (Ginn et al. 2017; Barcellos et al. 2018; Chen et al. 2018).

4 Conclusions

Mottles (or discrete zones of Fe-enriched and Fe-depleted soil) are a common occurrence in uplands soils of humid regions. In a soil profile with depth-dependent sequence of Fe-enriched and Fe-depleted Bt horizons, we found Fe-enriched zones primarily had a Fe mineral composition dominated by hematite and goethite, whereas in Fe-depleted zones, Fe was concentrated in aluminosilicates or low-crystallinity goethite. The persistence of low-crystallinity Fe phases in the Fe-depleted zones suggests re-precipitation events may not be limited to the Fe-enriched zones and active Fe redox cycling—rather than unidirectional Fe reduction—is likely in the Fe-depleted horizons. More pronounced is our finding that Fe phase crystallinity increases with depth in the Fe-enriched zones and low-crystallinity Fe(III) oxides are more abundant

at the top of Bt horizons in the Fe-depleted zones. Near-surface horizons that are highly enriched in OM are frequently found to have lower crystalline Fe phases than subsoils; however, here, we find this phenomenon extends well below surface horizons. Indeed, our evidence suggests that a decreasing Fe crystallinity with depth may occur in Bt horizon (~50–200 cm) even without high OM concentrations. Furthermore, the presence of low-crystallinity Fe(III) oxides in the upper Bt horizons suggest these horizons may have a greater sorption capacity for nutrients (e.g., P, N) or OM and greater ability to sustain anaerobic microbial Fe reduction than previously understood.

Acknowledgements Gratitude is expressed to the National Science Foundation for financial support of the research: NSF grants EAR-1331846 and EAR-1451508. We thank Jared Wilmoth for his assistance with Mössbauer analysis.

References

- Bacon AR (2014) Pedogenesis and anthropogenesis on the Southern Piedmont. Ph.D. thesis, Duke University
- Bacon AR, Richter DD, Bierman PR, Rood DH (2012) Coupling meteoric ^{10}Be with pedogenic losses of ^9Be to improve soil residence time estimates on an ancient North American interfluvium. *Geology* 40:847–850
- Bao H, Koch PL (1999) Oxygen isotope fractionation in ferric oxide-water systems: low temperature synthesis. *Geochim Cosmochim Acta* 63:599–613
- Barcellos D, Cyle KT, Thompson A (2018) Faster redox fluctuations can lead to higher iron reduction rates in humid forest soils. *Biogeochemistry* 137(3):367–378
- Bonneville S, Van Cappellen P, Behrends T (2004) Microbial reduction of iron (III) oxyhydroxides: effects of mineral solubility and availability. *Chem Geol* 212:255–268
- Bonneville S, Behrends T, Van Cappellen P (2009) Solubility and dissimilatory reduction kinetics of iron(III) oxyhydroxides: a linear free energy relationship. *Geochim Cosmochim Acta* 73:5273–5282
- Borch T, Kretzschmar R, Kappler A, Cappellen PV, Ginder-Vogel M, Voegelin A, Campbell K (2010) Biogeochemical redox processes and their impact on contaminant dynamics. *Environ Sci Technol* 44(1):15–23
- Buettner SW, Kramer MG, Chadwick OA, Thompson A (2014) Mobilization of colloidal carbon during iron reduction in basaltic soils. *Geoderma* 221–222:139–145
- Chadwick OA, Brimhall GH, Hendricks DM (1990) From a black to a gray box—a mass balance interpretation of pedogenesis. *Geomorphology* 3:369–390
- Chen C, Thompson A (2018) Ferrous iron oxidation under varying $p\text{O}_2$ levels: the effect of Fe(III)/Al(III) oxide minerals and organic matter. *Environ Sci Technol* 52(2):597–606
- Chen C, Dynes J, Wang J, Sparks DL (2014) Properties of Fe-organic matter associations via coprecipitation versus adsorption. *Environ Sci Technol* 48(23):13751–13759
- Chen C, Kukkadapu R, Sparks DL (2015) Influence of coprecipitated organic matter on $\text{Fe}^{2+}_{(\text{aq})}$ -catalyzed transformation of ferrihydrite: implications for carbon dynamics. *Environ Sci Technol* 49:10927–10936
- Chen C, Kukkadapu RK, Lazareva O, Sparks DL (2017) Solid-phase Fe speciation along the vertical redox gradients in floodplains using XAS and Mössbauer spectroscopies. *Environ Sci Technol* 51(14):7903–7912
- Chen C, Meile C, Wilmoth J, Barcellos D, Thompson A (2018) Influence of $p\text{O}_2$ on iron redox cycling and anaerobic organic carbon mineralization in a humid tropical forest soil. *Environ Sci Technol*. <https://doi.org/10.1021/acs.est.8b01368>
- Cheng YQ, Yang LZ, Cao ZH, Ci E, Yin S (2009) Chronosequential changes of selected pedogenic properties in paddy soils as compared with non-paddy soils. *Geoderma* 151:31–41
- Cheng L, Zhu J, Chen G, Zheng X, Oh NH, Ruffly TW, Richter DB, Hu S (2010) Atmospheric CO_2 enrichment facilitates cation release from soil. *Ecol Lett* 13:284–291
- Cismasu AC, MarcMichel F, Patricia Teaciuc A, Brown GE (2014) Properties of impurity-bearing ferrihydrite III. Effects of Si on the structure of 2-line ferrihydrite. *Geochim Cosmochim Acta* 133:168–185
- Cornell RM, Schwertmann U (2003) The Iron oxides: structure, properties, reactions, occurrences, and uses. Wiley-VCH Verlag GmbH, Weinheim
- Dubinsky EA, Silver WL, Firestone MK (2010) Tropical forest soil microbial communities couple iron and carbon biogeochemistry. *Ecology* 91:2604–2612
- Dyar MD, Grover TW, Rice JM, Guidotti CV (1987) Presence of ferric iron and octahedral ferrous ordering in biotites from schists: implications for garnet-biotite geothermometry. *Geol Soc Am Abstr Programs* 19:650
- Dyer LG, Chapman KW, English P, Saunders M, Richmond WR (2012) Insights into the crystal and aggregate structure of Fe^{3+} oxide/silica coprecipitates. *Am Mineral* 97(1):63–69
- Eusterhues K, Wagner FE, Häusler W, Hanzlik M, Knicker H, Totsche KU, Kögel-Knabner I, Schwertmann U (2008) Characterization of ferrihydrite-soil organic matter coprecipitates by X-ray diffraction and Mössbauer spectroscopy. *Environ Sci Technol* 42:7891–7897
- Fimmen RL, DB Richter D, Vasudevan D et al (2008) Rhizogenic Fe–C redox cycling: a hypothetical biogeochemical mechanism that drives crustal weathering in upland soils. *Biogeochemistry* 87:127–141
- Fysh SA, Cashion JD, Clark PE (1983) Mössbauer-effect studies of iron in kaolinite. 1. Structural iron. *Clay Clay Miner* 31:285–292
- Ginn BR, Meile C, Wilmoth J, Tang Y, Thompson A (2017) Rapid iron reduction rates are stimulated by high-amplitude redox fluctuations in a tropical forest soil. *Environ Sci Technol* 51(6):3250–3259
- Greenwood NN, Gibb TC (1971) Mössbauer spectroscopy. Chapman and Hall, London
- Hall SJ, Lipzin DL, DeAngelis K, Buss H, Silver WL (2016a) Drivers and patterns of iron redox cycling from surface to bedrock in a deep tropical forest soil: a new conceptual model. *Biogeochemistry* 130:177–190
- Hall SJ, Silver WL, Timokhin VI, Hammel KE (2016b) Iron addition to soil specifically stabilized lignin. *Soil Biol Biochem* 98:95–98
- Hassellöv M, von der Kammer F (2008) Iron oxides as geochemical nanovectors for metal transport in soil–river systems. *Elements* 4:401–406
- Hossner L et al (1996) Dissolution for total elemental analysis. In: Sparks DL et al (eds) *Methods of soil analysis, Part 3—chemical methods*. American Society of Agronomy, Madison, pp 49–64
- Jacobs PM, West LT, Shaw JN (2002) Redoximorphic features as indicators of seasonal saturation, Lowndes County, Georgia. *Soil Sci Soc Am J* 66:315–323
- Janot C, Gibert H, Tobias C (1973) Caractérisation des kaolinites ferrifères par spectrométrie Mössbauer. *Bull Soc Fr Mineral Cristallogr* 96:281–291
- Jones AM, Collins RN, Rose J, Waite TD (2009) The effect of silica and natural organic matter on the Fe(II)-catalysed transformation and reactivity of Fe(III) minerals. *Geochim Cosmochim Acta* 73(15):4409–4422

- Kämpf N, Schwertmann U (1983) Goethite and hematite in a climosequence in southern Brazil and their application in classification of kaolinitic soils. *Geoderma* 29:27–39
- Kölbl A, Schad P, Jahn R, Amelung W, Bannert A, Cao ZH, Fiedler S, Kalbitz K, Lehnendorff E, Müller-Niggemann C, Schloter M, Schwark L, Vogelsang V, Wissing L, Kögel-Knabner I (2014) Accelerated soil formation due to paddy management on marshlands (Zhejiang Province, China). *Geoderma* 228–229:67–89
- Kukkadapu RK, Zachara JM, Fredrickson JK, McKinley JP, Kennedy DW, Smith SC, Dong HL (2006) Reductive biotransformation of Fe in shale–limestone saprolite containing Fe(III) oxides and Fe(II)/Fe(III) phyllosilicates. *Geochim Cosmochim Acta* 70:3662–3676
- Kurtz AC, Derry LA, Chadwick OA, Alfano MJ (2000) Refractory element mobility in volcanic soils. *Geology* 28:683–686
- Lalonde AE, Rancourt DG, Ping JY (1998) Accuracy of ferric/ferrous determinations in micas: a comparison of Mössbauer spectroscopy and the Pratt and Wilson wet-chemical methods. *Hyperfine Interact* 117:175–204
- Lalonde K, Mucci A, Quillet A, Gélinas Y (2012) Preservation of organic matter in sediments promoted by iron. *Nature* 483:198–200
- Langmuir D (1971) Particle size effect on the reaction goethite = hematite + water. *Am J Sci* 271:147–156
- Li J, Richter DD, Mendoza A, Heine P (2008) Four-decade responses of soil trace elements to an aggrading old-field forest: B, Mn, Zn, Cu, and Fe. *Ecology* 89(10):2911–2923
- Li Y, Yu S, Strong J, Wang H (2012) Are the biogeochemical cycles of carbon, nitrogen, sulfur, and phosphorus driven by the “Fe-III-Fe-II redox wheel” in dynamic redox environments? *J Soils Sediments* 12:683
- Lindbo DL, Stolt MH, Vepraskas MJ (2010) Redoximorphic features. In: Interpretation of micromorphological features of soils and regoliths, pp 129–147
- Lovley DR (1995) Microbial reduction of iron, manganese and other metals. *Adv Agron* 54:175–231
- Lovley DR, Holmes DE, Nevin KP (2004) Dissimilatory Fe(III) and Mn(IV) reduction. *Adv Microb Physiol* 49:219–286
- Mansfeldt T, Schuth S, Häusler W, Wagner F, Kaufhold S, Overesch M (2012) Iron oxide mineralogy and stable iron isotope composition in a Gleysol with petroglycic properties. *J Soils Sediments* 12:97–114
- Markewitz D, Richter DD (2000) Long-term soil potassium availability from a Kanhapludult to an aggrading loblolly pine ecosystem. *For Ecol Manag* 130:109–129
- Markewitz D, Richter DD, Allen HL, Urrego JB (1998) Three decades of observed soil acidification at the Calhoun Experimental Forest: has acid rain made a difference? *Soil Sci Soc Am J* 62:1428–1439
- Mayer TD, Jarrell WM (1996) Formation and stability of iron(II) oxidation products under natural concentrations of dissolved silica. *Water Res* 30:1208–1214
- Merino E (1984) Survey of geochemical self-patterning phenomena. In: Nicolis G, Baras F (eds) *Chemical instabilities*. D. Reidel Publishing Company, Dordrecht, pp 305–328
- Mikutta C, Mikutta R, Bonneville S, Wagner F, Voegelin A, Christl I, Kretzschmar R (2008) Synthetic coprecipitates of exopolysaccharides and ferrihydrite. Part I: characterization. *Geochim Cosmochim Acta* 72:1111–1127
- Mobley ML, Lajtha K, Kramer MG, Bacon AR, Heine PR, Richter DD (2015) Surficial gains and subsoil losses of soil carbon and nitrogen during secondary forest development. *Glob Change Biol* 21:986–996
- Moore DM, Reynolds RC (1997) X-ray diffraction and the identification and analysis of clay minerals. Oxford University Press, Oxford, p 378
- Murad E, Cashion J (2004) Mössbauer spectroscopy of environmental materials and their industrial utilization. Kluwer Academic Publishers Group, Norwell
- Murad E, Schwertmann U (1983) The influence of aluminium substitution and crystallinity on the Mössbauer spectra of goethite. *Clay Miner* 18:301–312
- Noël V, Marchand C, Juillot F, Ona-Nguema G, Viollier E, Marakovic G, Olivi L, Delbes L, Gelebart F, Morin G (2014) EXAFS analysis of iron cycling in mangrove sediments downstream a lateritized ultramafic watershed (Vavouto Bay, New Caledonia). *Geochim Cosmochim Acta* 136:211–228
- Peretyazhko T, Sposito G (2005) Iron (III) reduction and phosphorous solubilization in humid tropical forest soils. *Geochim Cosmochim Acta* 69:3643–3652
- Postma D (1993) The reactivity of iron oxides in sediments: a kinetic approach. *Geochim Cosmochim Acta* 57:5027–5034
- Quénard L, Samouëlian A, Laroche B, Cornu S (2011) Lessivage as a major process of soil formation: a revisitation of existing data. *Geoderma* 167–168:135–147
- Rancourt DG (1998) Mössbauer spectroscopy in clay science. *Hyperfine Interact* 117:3–38
- Rancourt DG, Ping JY (1991) Voigt-based methods for arbitrary-shape static hyperfine parameter distributions in Mössbauer spectroscopy. *Nucl Instrum Methods Phys Res Sect B Beam Interact Mater At* 58: 85–97
- Richter DD, Markewitz D (2001) Understanding soil change. Cambridge University Press, Cambridge
- Richter DD, Markewitz D, Wells CG, Allen HL, April R, Heine PR, Urrego B (1994) Soil chemical change during three decades in an old-field loblolly pine (*Pinus taeda* L.) ecosystem. *Ecology* 75(5): 1463–1473
- Richter DD, Markewitz D, Heine PR, Jin V, Raikes J, Tian K, Wells CG (2000) Legacies of agriculture and forest regrowth in the nitrogen of old-field soils. *Forest Ecol Manag* 138(1–3):233–248
- Richter DD, Oh NH, Fimmen R, Jackson J (2007) The rhizosphere and soil formation. In: Cardon ZG, Whitbeck JL (eds) *The rhizosphere*. Academic Press, Cambridge, pp 1799–1200
- Roden E, Wetzel R (1996) Organic carbon oxidation and suppression of methane production by microbial Fe(III) oxide reduction in vegetated and unvegetated freshwater wetland sediments. *Limnol Oceanogr* 41:1733–1748
- Roden EE, Wetzel RG (2002) Kinetics of microbial Fe(III) oxide reduction in freshwater wetland sediments. *Limnol Oceanogr* 47:198–211
- Roden EE, Zachara JM (1996) Microbial reduction of crystalline iron (III) oxides: influence of oxide surface area and potential for cell growth. *Environ Sci Technol* 30:1618–1628
- Schroeder PA (2018) *Clays in the critical zone*. Cambridge University Press, Online ISBN: 9781316480083, 252 pp
- Schroeder PA, Kim JG, Melear ND (1997) Mineralogical and textural criteria for recognizing remnant Cenozoic deposits on the Piedmont: evidence from Sparta and Greene County, Georgia, U.S.A. *Sediment Geol* 108:195–206
- Schroeder PA, Pruett RJ, Melear ND (2004) Crystal-chemical changes in an oxidative weathering front in a middle Georgia kaolin deposit. *Clay Clay Miner* 52:212–220
- Schulz M, Stonestrom D, Lawrence C, Bullen T, Fitzpatrick J, Kyker-Snowman E, Manning J, Mnich M (2016) Structured heterogeneity in a marine terrace chronosequence: upland mottling. *Vadose Zone J* 15(2). <https://doi.org/10.2136/vzj2015.07.0102>
- Schwertmann U (1985) The effect of pedogenic environments on iron oxide minerals. *Advances in soil science*, vol 1. Springer-Verlag, New York Inc., New York, pp 171–180
- Schwertmann U, Cornell RM (1991) Iron oxides in the laboratory—preparation and characterization. VCH Verlagsgesellschaft, Weinheim
- Schwertmann U, Taylor RM (1989) Iron oxides. In: Dixon JB, Weed SB, Kittrick JA, Milford MH, White JL (eds) *Minerals in soil environments*. Soil Science Society of America, Madison, pp 145–180

- Schwertmann U, Thalmann H (1976) The influence of Fe(II), Si and pH on the formation of lepidocrocite and ferrihydrite during oxidation of aqueous FeCl₂ solutions. *Clay Mineral* 11:189–200
- Schwertmann U, Friedl J, Kyek A (2004) Formation and properties of a continuous crystallinity series of synthetic ferrihydrites (2- to 6-line) and their relation to FeOOH forms. *Clay Clay Miner* 52:221–226
- Schwertmann U, Wagner F, Knicker H (2005) Ferrihydrite–humic associations. *Soil Sci Soc Am J* 69:1009–1015
- Taylor KG, Konhauser KO (2011) Iron in earth surface systems: a major player in chemical and biological processes. *Elements* 7:83–88
- Thamdrup B (2000) Bacterial manganese and iron reduction in aquatic sediments. In: Schink B (ed) *Advances in microbial ecology*. Springer, Boston, pp 41–84
- Thompson A, Chadwick OA, Boman S, Chorover J (2006a) Colloid mobilization during soil iron redox oscillations. *Environ Sci Technol* 40(18):5743–5749
- Thompson A, Chadwick OA, Rancourt DG, Chorover J (2006b) Iron-oxide crystallinity increases during soil redox oscillations. *Geochim Cosmochim Acta* 70:1710–1727
- Thompson A, Chadwick OA, Rancourt DG, Chorover J (2011) Iron solid-phase differentiation along a redox gradient in basaltic soils. *Geochim Cosmochim Acta* 75(1):119–133
- Torrent J, Guzman R, Parra MA (1982) Influence of relative humidity on the crystallization of Fe(III) oxides from ferrihydrite. *Clay Clay Miner* 30:337–340
- Trolard F, Tardy Y (1987) The stabilities of gibbsite, boehmite, aluminous goethites and aluminous hematites in bauxites, ferricretes and laterites as a function of water activity, temperature and particle size. *Geochim Cosmochim Acta* 51:945–957
- Veneman PLM, Spokas LA, Lindbo DL (1998) Soil moisture and redoximorphic features: a historical perspective. In: Rabenhorst MC, Bell JC, McDaniel PA (eds) *Quantifying soil hydromorphology*, SSSA Spec. Publ. 54. SSSA, Madison, pp 1–23
- Vogelsang V, Kaiser K, Wagner FE, Jahn R, Fiedler S (2016) Transformation of clay-sized minerals in soils exposed to prolonged regular alternation of redox conditions. *Geoderma* 278:40–48
- Weber KA, Achenbach LA, Coates JD (2006) Microorganisms pumping iron: anaerobic microbial iron oxidation and reduction. *Nat Rev Microbiol* 4:752–764
- Wiederhold JG, Teutsch N, Kraemer SM, Halliday AN, Kretzschmar R (2007) Iron isotope fractionation during pedogenesis in redoximorphic soils. *Soil Sci Soc Am J* 71:1840–1850
- Winkler P, Kaiser K, Thompson A, Kalbitz K, Fiedler S, Jahn R (2018) Contrasting evolution of iron phase composition in soils exposed to redox fluctuations. *Geochimica et Cosmochimica Acta* 235:89–102
- Yang WH, Liptzin D (2015) High potential for iron reduction in upland soils. *Ecology* 96:2015–2020
- Yapp CL (1983) Effects of AlOOH-FeOOH solid solution on goethite-hematite equilibrium. *Clay Clay Miner* 31:239–240
- Zhang MK, Wilson MJ, He ZL (1998) Iron oxides and their relations to colors in some soils of southern China. *Pedosphere* 8:53–58
- Zhang Y, Lin X, Werner W (2003) The effect of soil flooding on the transformation of Fe oxides and the adsorption/desorption behavior of phosphate. *J Plant Nutr Soil Sci* 166:68–75